

GT2011-4) %\$(

VALIDATION OF AN IGNITION AND FLAME PROPAGATION MODEL FOR MULTIPHASE FLOWS

J. M. Boyde*, P. Le Clercq, M. Di Domenico, M. Rachner, G. C. Gebel, T. Mosbach, M. Aigner

German Aerospace Center (DLR)
Institute of Combustion Technology
Pfaffenwaldring 38 - 40, 70569 Stuttgart, Germany
E-Mail*: jan.boyde@dlr.de

ABSTRACT

This paper presents a numerical investigation of a generic lab scale combustor with focus on the ignition characteristics. The test case has been examined thoroughly in a comprehensive measurement campaign to provide a detailed set of boundary conditions and a profound data base of results. The experimental set-up comprises five parallel-aligned mono-disperse droplet chains which are ignited, using a focused laser beam. One aspect of the experimental study is the ignitability with respect to the imposed boundary conditions. The second covers the growth and the propagation of the flame after the establishment of an initial kernel. The outcome of the numerical simulations is compared to the experimental results which allows an in-depth assessment of the employed numerical models. The chemistry and, thus, the flame propagation behavior is captured by a turbulent flame speed closure approach with an adaptation to render the model suitable to multiphase flows. For the dispersed phase a Lagrangian particle tracking scheme is employed in combination with a continuous thermodynamics fuel model for the evaporation. The overall good agreement demonstrates the capability of a multiphase flow CFD solver in the field of ignition modeling.

Keywords: Flame Propagation, Ignition, Multiphase flows, Turbulent Flame Speed Closure, Droplet Evaporation, Continuous Thermodynamics, Evaporation

NOMENCLATURE

A	Model constant.
c	Flame progress variable.
c_p	Specific heat capacity at constant pressure
$C_{ign}/C, C^*$	Model constant / Coefficients.
D, D_d	Diffusivity / Diameter of the droplet.
E_e, E_h	Energy for the evaporation / Energy for the heating.
f_e	Fraction of vapor.
h, H_e	Specific enthalpy / Vaporization enthalpy.
\dot{m}	Mass Flow.
r, l_s, l_r	Radius / Spark Height / Recirculation Length.
Sc	Schmidt Number.
S_L, S_T	Laminar / Turbulent flame speed.
t_i	Ignition delay time.
T	Temperature.
u, v	Velocity.
u', l_t	Isotropic velocity fluctuation / Integral length scale.
U_d, U_f	Velocity droplet / Velocity fluid.
\dot{w}	Source term.
x	Space variable.
Y	Mass fraction.
μ_g, ν	Dynamic viscosity / Kinematic viscosity.
θ, ω, γ	Gamma-distribution parameter.
ϕ	Equivalence ratio.
ρ, ρ_l	Density / Density of the liquid.
Φ_{max}	Maximum attainable local mass fraction of CO ₂ .
χ	Thermal Diffusivity.

* Address all correspondence to this author.

INTRODUCTION

The description of the flame propagation in a combustion chamber still poses a challenge, which has been investigated in the combustion community for a long time. The first study, related to the ignitability of a jet flame has been accomplished almost 30 years ago, by Birch et al. [1]. The main applications are found within transient processes which require detailed information about the spatial and temporal development of the reaction zone. Light off, altitude relight and sudden changes in load during the flight cycle constitute examples, which need to be modeled with respect to their transient nature. Since experiments concerning the ignitability of an aircraft engine combustor are associated with high costs and are constrained to the end of the engine design cycle, a continuous need exists to improve the design process at an earlier stage. Thus, a large interest persists in developing modeling strategies for the initial flame kernel evolution. Experiments designed to advance the development of numerical tools which are able to capture ignition events are recently provided by Ahmed et al. and Mastorakos et al. [2–5]. This is significantly supporting the understanding and accuracy of transient solver strategies as proven by several papers [6, 7]. However, none of the papers so far extends to include multiphase physics, being the physical groundwork of modern combustion engines, since test cases of ignition phenomena on this field are still scarce. Hence, the results presented in this study are of scientific interest with the focus on the question of ignitability. Through the incorporation of a continuous and a discrete phase, it takes the relevance of this investigation one step closer to a real combustion chamber application. The new aspect which arises in the modeling of multiphase flows is the prediction of the fuel evaporation. Another key factor for the probability of the establishment of a fully developed flame are the initial conditions which are assumed for the numerical treatment of the ignition procedure. In the lab-configuration, the employed device to trigger the ignition is a laser pulse, for which the fundamental characteristics are discussed. With the available experimental data, the numerical set-up is validated. The paper is structured as follows: First, we provide a description of the test case. Afterwards the main models used in the simulations are covered. Subsequently, the two challenges, stemming from the multiphase flow physics, namely the spontaneous vapor generation and the evaporation characteristics of the flow are discussed and the results compared to the experiment.

TEST CASE DESCRIPTION

The investigated test case consists of a rectangular flow channel mounted with a fuel injector as depicted in Fig. (1). The channel cross sectional area amounts to $62 \times 10^{-4} \text{ m}^2$ with a total length of 1 m. In the course of the simulations the channel length is curtailed to 490 mm as above approximately 400 mm with respect to the channel top no experimental data was measured.

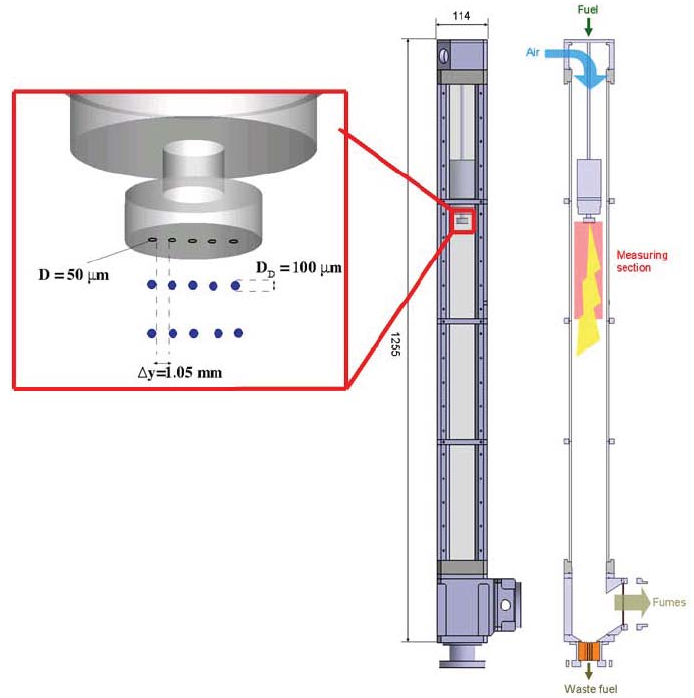


FIGURE 1. Sketch of the test case. Air inflowing from the top of the channel with the fuel droplets emerging from the injector in the upper half. The laser ignition zone is located right underneath the injector plane. The left hand side shows the injector configuration in detail.

Through the unambiguous design, the intention was to minimize influences stemming from the geometry. A fuel injector is embedded in the middle of the channel extending from the channel inlet to 290 mm axial position. From the fuel injector five parallel mono-dispersed droplets with a diameter of $100 \mu\text{m}$ emerge which are ignited at 10 mm (300 mm total axial position) distance from the injector plane. The ignition is carried out with a frequency-doubled Nd:YAG laser which is able to produce pulse energies up to 400 mJ in single shot mode. The laser focal point is directed into the droplet chain next to the laser beam incident direction. In the course of the examination, PLIF measurements of the fuel and OH distribution were accomplished. Additional measurements were performed to capture the broadband luminosity. Two schematic representations of the experimental set-up are presented in Fig. (2). For a detailed description of the measurement devices and techniques, the reader is referred to Boyde et al. [8]. The fuel inflow rates can be varied, ranging from 60 slm (standard liter per minute) to 600 slm, whereas the fuel mass rate can be prescribed from 1.9 g/min up to over 6 g/min.

By means of this configuration, the flame propagation and simultaneous flame growth were investigated experimentally. Additionally, the fuel vapor development was captured which allows an insight into the processes governing the flame behavior. The

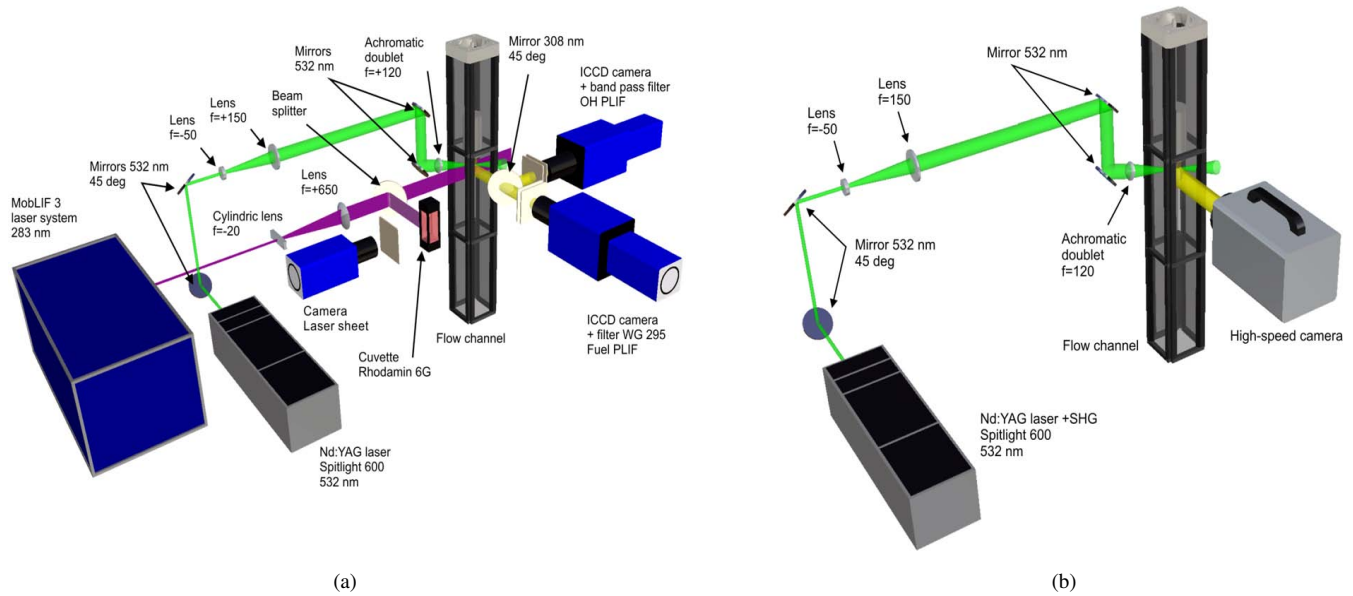


FIGURE 2. Schematics of the experimental set-up. (a) Devices and alignment for the simultaneous planar laser-induced fluorescence (PLIF) measurements of the fuel and OH distribution. (b) Devices and alignment for the high-speed imaging of the broadband luminosity.

data from broadband luminosity measurements provides further details about the exact location of the flame and the flame kernel evolution. Combined analysis of both data sets yield a good spatial and temporal resolution of the reaction zones. Furthermore, measurements concerning the ignitability of the mixture were accomplished which were conveyed in an ignition map, also representing an objective of the numerical simulations.

NUMERICAL SET-UP

Flow Solver

The numerical simulations carried out in the scope of this study employ the CFD code THETA, developed at the DLR. For stationary calculations the SIMPLE method was utilized, as detailed in Ferziger [9]. Transient calculations were run with a projection method as pressure-velocity coupling scheme [9]. The temporal discretization was accomplished with a three point backwards method yielding second order accuracy. For the turbulent closure a standard $k-\epsilon$ turbulence model [10] with wall functions was incorporated. The equations are discretized in a vertex-centered manner and solved by a Bi-Conjugate Gradient Stabilized (BiCGStab [11]) method. Second-order upwind and central schemes are used for convective and diffusive terms respectively.

Combustion Model Equations

For the inclusion of the combustion processes, a model based on the turbulent flame speed closure model, hereafter named TFC-model, originally developed by Zimont [12], was employed. The

TFC model has a superior nature for this kind of study as it is designed to capture the flame propagation accurately. Since its formulation is derived from the laminar flame speed, it enables an excellent description of the flame spreading behavior. The TFC model is based on a flame progress variable, c , for which the basic transport equation reads:

$$\frac{\partial}{\partial t}(\bar{\rho}\bar{c}) + \frac{\partial}{\partial x_k}(\bar{\rho}\tilde{u}_k\bar{c}) = \frac{\partial}{\partial x_k} \left(\bar{\rho} \frac{\nu_t}{Sc_c} \frac{\partial \bar{c}}{\partial x_k} \right) + \bar{w}_c \quad (1)$$

The source \bar{w}_c term will be quantified in the further course of this paragraph. Note that the diffusion term only contains the contribution from the turbulent diffusion ν_t , as the laminar diffusion part is contained intrinsically by the laminar flame speed, as discussed, e.g. by Durand [13]. The expression Sc_c corresponds to the Schmidt Number which is 0.7 in all simulations. The model has been widely used and applied by numerous researchers [14], [15] to which the reader is referred to, for more details on the derivation or for a more thorough validation background of the model itself. For the sake of completeness, the gist shall be recapitulated in the following with a subsequent description of the multiphase flow adaptation. The afore mentioned transport equation allows a basic flame description within a homogeneous premixed environment. For a more complex flame regime, three other transport equations are necessary, to account for all occurring physical phenomena. The second equation relates to the fuel vapor transport:

$$\frac{\partial}{\partial t} (\bar{\rho} \tilde{Y}_f) + \frac{\partial}{\partial x_k} (\bar{\rho} \tilde{u}_k \tilde{Y}_f) = \frac{\partial}{\partial x_k} \left(\bar{\rho} D_{Y_f} \frac{\partial \tilde{Y}_f}{\partial x_k} \right) + \bar{w}_f \quad (2)$$

The source term \bar{w}_f comprises the generation of additional fuel vapor through the evaporation of the liquid phase. D_{Y_f} represents the diffusion coefficient of the fuel, which corresponds to:

$$D_{Y_f} = \frac{\nu}{Sc_f} + \frac{\nu_t}{Sc_{t_f}} \quad (3)$$

with the constants Sc_f and Sc_{t_f} being also 0.7. ν and ν_t represent the laminar and turbulent viscosity respectively. In order to allow non-adiabatic effects to be captured, the specific enthalpy needs to be accounted for by a separate transport equation, which gives:

$$\frac{\partial}{\partial t} (\bar{\rho} \tilde{h}) + \frac{\partial}{\partial x_k} (\bar{\rho} \tilde{u}_k \tilde{h}) = \frac{\partial}{\partial x_k} \left(\bar{\rho} D_h \frac{\partial \tilde{h}}{\partial x_k} \right) + \bar{w}_h \quad (4)$$

with $D_h = D_{Y_f}$. The last transport equation represents an extension necessary for the multiphase flow regime. As the generation of fuel vapor constitutes a new environment for the TFC-model, this needs to be considered in the model formulation. In a lean mixture, the increase of the fuel vapor concentration will lead to a reduction of the flame progress variable, as the evaporated fuel vapor is not fully burned yet. Hence, by incorporating a transport equation for the exhaust gas species CO_2 , stemming from the progress of the reaction, a comparison can be accomplished of the current local state of the reaction to the local amount of exhaust gas. The fourth transport equation, thus, reads:

$$\frac{\partial}{\partial t} (\bar{\rho} \tilde{Y}_{CO_2}) + \frac{\partial}{\partial x_k} (\bar{\rho} \tilde{u}_k \tilde{Y}_{CO_2}) = \frac{\partial}{\partial x_k} \left(\bar{\rho} D_{Y_{CO_2}} \frac{\partial \tilde{Y}_{CO_2}}{\partial x_k} \right) + \bar{w}_{CO_2} \quad (5)$$

with $D_{CO_2} = D_{Y_f}$. The source term \bar{w}_{CO_2} is coupled to changes in the flame progress variable which is detailed later in this section. At first, the source term of the flame progress variable shall be specified.

$$\bar{w}_c = \rho_u S_T |\nabla \tilde{c}| + C_{ign} \bar{\rho} \frac{1}{t_i} \quad (6)$$

The first part of Eq. (6) relates to the standard implementation of the TFC model. It links the flame progress variable to the local turbulent flame speed and to the gradient of the flame progress

variable. The expression employed for the turbulent flame speed was first derived by Zimont et al. [12] and reads:

$$S_T = Au'^{3/4} S_L^{1/2} \chi_u^{-1/4} l_t^{1/4}. \quad (7)$$

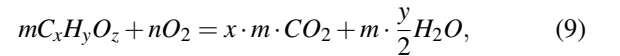
An additional condition is imposed through

$$S_T = \max(S_T, S_L), \quad (8)$$

which restores the laminar flame speed in regions with insufficient turbulence. Note that the quenching term G present in the original work of Zimont [12] has been omitted as the occurring turbulence is of moderate magnitude. In Eq. 7, u' represents the isotropic velocity fluctuations, χ_u denotes the thermal diffusivity at unburned conditions and l_t resembles the integral length scale. S_L stands for the laminar flame speed and A is a model constant which is 0.52, see Zimont et al. [12], in all simulations.

The second contribution $C_{ign} \bar{\rho} \frac{1}{t_i}$ to the source term stems from the laser pulse event. C_{ign} is a model constant which is 1.0 throughout this paper. In the original TFC model no formulation to trigger the ignition is present, hence, artificial assumptions are required to initiate a flame kernel. Opposed to that, by coupling the flame progress variable to the auto-ignition characteristics of the mixture a more natural and physical correct implementation is derived. Details of the derivation are given in Boyde et al. [7]. The basic concept of the auto-ignition submodule is an integral technique, which corresponds to the assumption, that once the local ignition delay time has passed, the flame is in a fully burned state. Consequently, by evaluating the auto-ignition time at each time step the contribution to the flame progress can be derived.

Additionally a limiter has been introduced which accounts for evaporation effects. The local mixture is evaluated in terms of being either lean or rich. This can be done by using a single step global reaction for the fuel in the shape of:



which yields for the stoichiometric ratio:

$$n_{st} = \frac{1}{x + 1/4y - z/2}. \quad (10)$$

By these means, the current composition can be distinguished through $X_f/X_{O_2} \leq n_{st}$. In case the composition is below the stoichiometric mixture fraction $X_f/X_{O_2} < n_{st}$, a raise of the fuel vapor content will lead to a reduction of the flame progress,

as the fraction of burned fuel with respect to the amount of burnable fuel has reduced. Therefore, at the end of each time an evaluation is accomplished whether the local flame progress is level with the amount of burned fuel, represented by Y_{CO_2} to the amount of burnable fuel, resembled by Φ_{max} . Φ_{max} corresponds to the maximum local mass fraction of CO_2 , which is computed by virtue of Eq. (9). This is more consistent with the definition of the flame progress variable as a measure of the ratio of the current burned fuel to the maximum burnable fuel. For a local fuel rich zone, the additional limiter has no effect as the oxygen controls the maximum reaction rate.

The source term of the transport equation for CO_2 is coupled to the flame progress variable. Consequently, for \bar{w}_{CO_2} we can write:

$$\bar{w}_{CO_2} = \bar{w}_c \cdot \Phi_{max}. \quad (11)$$

The handling of the exhaust gas CO_2 enables a further advantage. The variables of state of the mixture can be correlated to the exhaust gas mass fraction by means of computing the temperature in accordance to the local mixture composition and enthalpy. In the original version of the TFC model, the temperature constituted a function of the flame progress and the adiabatic flame temperature. Hence, by omitting intermediate species, a good approximation of the temperature in the domain is obtained, through:

$$h(T) = h_c + \int_{T_c}^T c_p \cdot dT \quad (12)$$

For c_p the mass weighted average of all species is substituted and the index c denotes cold flow quantities.

The density is, subsequently, derived by solving the equation of state. One further aspect of the extension needs to be discussed. Formerly, the spreading of a region of burned gas within a stagnant environment was not coped with. By correlating the temperature with the mass fraction ratios, thus, quantities which exhibit a natural diffusion behavior, a more independent formulation is gained, which helps the physical integrity of the model. Two unresolved tasks remain for the closure of the model. The laminar flame speed needs to be provided for the source term in Eq. (6) and, furthermore, an expression for the ignition delay time needs to be found, for the auto-ignition contribution. Both quantities are delivered to the model by polynomial expressions which have been validated in the course of this study and can be examined more thoroughly in Boyde [16]. The extracted coefficients and the structure of the curve can be found in Table 1.

Modeling of the liquid phase

For the dispersed phase, a Lagrangian particle tracking scheme is combined with a continuous thermodynamics model, hereafter termed CTM model, which mimics the fuel properties. Both schemes are part of the SPRAYSIM liquid phase solver which is developed at the DLR. The particles representing the droplets are treated in a two way coupling fashion, meaning that the liquid phase provides a source term to the gas phase and vice-versa. The turbulence-spray interaction is taken into account by using a droplet turbulence dispersion model based on the spectral reconstruction of local turbulent features [17].

The CTM model allows a more realistic treatment of the fuel properties as a multi-component fuel is considered to be composed of several chemical species which is more consistent with the real nature of complex fuels, see Fig. (3). A detailed description of the implementation of continuous thermodynamics in multiphase flow solvers is presented elsewhere. [18], [19], [20] The distribution for the Jet A-1 fuel in the simulation is presented in Table 2, which complies with experimentally determined characteristics of Jet A-1, see the work of Wahl [21] and which has been used successfully in other studies, e.g. Le Clercq et al. [22].

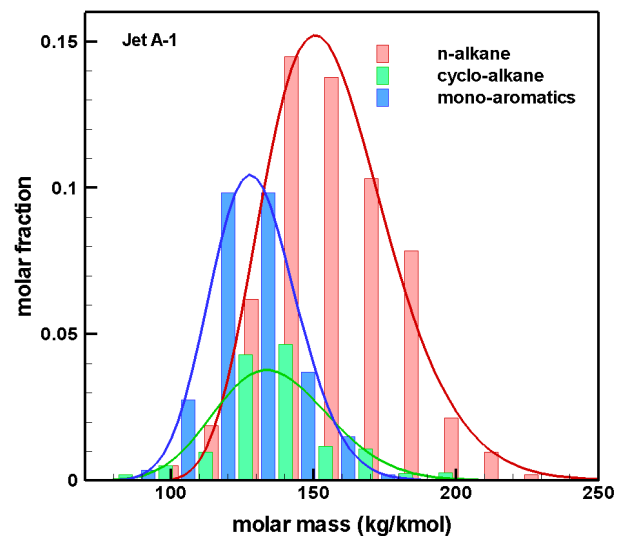


FIGURE 3. Molar fraction distribution for the different components of Jet A-1.

Coefficients	Laminar Flame Speed	Ignition Delay Time
General Form	$s_L = C_1 + C_2\phi + C_3\phi^2 + C_4\phi^3 + C_5\phi^4$	$t_i = C_1 + C_2\phi$
Correl. for C_i	$C_i = C_{i,1}^* + C_{i,2}^*T + C_{i,3}^*T^2 + C_{i,4}^*T^3$	$C_i = C_{i,1}^* + C_{i,2}^* \cdot 1/T + C_{i,3}^* \cdot 1/T^2 + C_{i,4}^* \cdot 1/T^3 + C_{i,5}^* \cdot 1/T^4$
Input	Note, T/300 in [K], p/1e5 in [Pa].	Note, T/1000 in [K], p/1e5 in [Pa].
Coefficients	$C_{1,1}^*$: 3.4296e0 $C_{1,2}^*$: -5.8142e0 $C_{1,3}^*$: 4.2813e0 $C_{1,4}^*$: -1.1513e0 $C_{2,1}^*$: -1.5388e1 $C_{2,2}^*$: 2.5354e1 $C_{2,3}^*$: -1.9929e1 $C_{2,4}^*$: 5.5862e0 $C_{3,1}^*$: 2.4746e1 $C_{3,2}^*$: -3.962e1 $C_{3,3}^*$: 3.3386e1 $C_{3,4}^*$: -9.2624e0 $C_{4,1}^*$: -1.6716e1 $C_{4,2}^*$: 2.6633e1 $C_{4,3}^*$: -2.3060e1 $C_{4,4}^*$: 6.3860e0 $C_{5,1}^*$: 3.9995e0 $C_{5,2}^*$: -6.4327e0 $C_{5,3}^*$: 5.5555e0 $C_{5,4}^*$: -1.5469e0	$C_{1,1}^*$: 9.90683e1 $C_{1,2}^*$: -6.27904e0 $C_{1,3}^*$: 1.49218e1 $C_{1,4}^*$: -1.57675e1 $C_{1,5}^*$: 6.25666e0 $C_{2,1}^*$: -1.19870e0 $C_{2,2}^*$: 7.64451e0 $C_{2,3}^*$: -1.82555e1 $C_{2,4}^*$: 1.93541e1 $C_{2,5}^*$: -7.68889e0

TABLE 1. Coefficients for the laminar flame speed and the auto-ignition time of n-Decane.

Composition of Jet A-1

composition	n-alkane	cyclo-alkane	mono-aromatics
x_j	0.5836	0.1342	0.2822
θ_j [g/mol]	157.0	136.7	129.7
σ_j [g/mol]	22.2	20.0	15.2
γ_j [g/mol]	80	0	0

TABLE 2. Parameters of the fitted Gamma-distributions for the CTM model.

Grid

The development of the grid for this test case was a delicate task. Small grid cells in the ignition zone constitute one major requirement for being able to accurately adjust the laser pulse zone. However, the requirement for the modeling of the liquid phase to have grid cells far larger than the droplet size, opposes the former. For this reason the grid cells in the part just below the injector are of adequate small size of about 0.25 mm, representing a compromise between the two demands. Nevertheless, smaller grid cells in the ignition zone would have been helpful for being able to prescribe the ignition zone volume even more precisely. Fig. (4) depicts an extract of the grid at the injector plane.

Another reason for choosing small grid cells in the vicinity of the injector is imposed by the very small distance between the injector holes. The distance amounts to 1.05 mm. It needs to be avoided that one grid cell has to account for two injector holes as the accuracy of the calculation would be hampered.

As the inlet velocity at the beginning of the channel only ranges

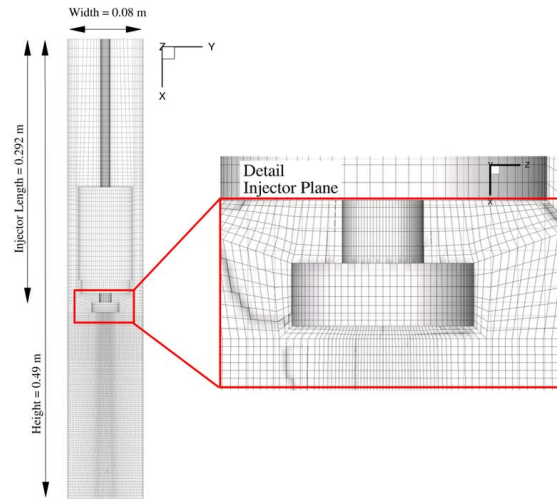


FIGURE 4. Numerical domain and injector grid design.

between 0.18 m/s to 1.79 m/s, the coarse discretization at the top of the channel is justified. In total, the number of cells is of the order of 450,000. This enables an efficient calculation with a URANS approach with the main features being well resolved. Regarding grid independency investigation, the cold flow simulation was carried out with three different grid set-ups. The first corresponds to the one used in all subsequent simulations. The second configuration constitutes a grid of coarser resolution which was able to provide accurate flow results as well. A third one which represents only a quarter section of the coarser grid, also resolved the flow field well. Hence, the grid, with respect to the flow field, can be regarded as of no influence towards the flow field outcome.

Air Velocity	Fuel Mass Flow	Fuel Type Liquid / Gaseous	Evaporation Fraction	Purpose
1.79 m/s	-	-	-	Cold Flow Field Validation
1.79 m/s	1.9 [g/min]	n-Decane / n-Decane	-	Flow Field with Droplets
1.0 m/s	2.5 [g/min]	n-Decane / n-Decane	0 %	Ignition Characteristics
1.0 m/s	2.5 [g/min]	n-Decane / n-Decane	50 %	Ignition Characteristics
0.36 - 1.79 m/s	4.0 [g/min] - 5.0 [g/min]	Jet A-1 / n-Decane	0 %	Ignition Map

TABLE 3. Boundary conditions for all investigated configurations.

Boundary Conditions

The calculations were carried out with the settings as listed in Table 3. In general, the boundary conditions imposed on the test case are:

- A bulk velocity inlet condition for the air inflow at the top of the domain is imposed.
- At the fuel inlet $x = 0.292$ m, which corresponds to the injector plane location, the droplet velocity which is derived by means of the continuity equation is prescribed.
- Side walls are modeled as adiabatic no slip boundaries.
- Temperature is set to 295 K for both inlets.

The measured mass flow in the experiment is homogeneously split on all five injector holes. The size assumed for all injected droplets is equal to $100 \mu\text{m}$ which is in good accordance with the experimental set-up in which the droplet size ranges between 96 - $100 \mu\text{m}$. Concerning the procedure which was adopted for all transient calculation involving an artificial laser pulse, the following steps were accomplished:

1. Steady state cold flow solution was computed without the liquid phase.
2. Steady state solution of the flow field including droplets was obtained.
3. The solver was set to transient mode. The flow field with the dispersed phase, modeled as parcels injected with the correct experimental frequency, was simulated until the overall solution reaches a quasi-steady behavior.
4. Laser pulse energy was imposed on the flow field. Ignition occurs.

These steps are necessary in order to optimize the required computational effort.

RESULTS

This section contains the outcome of this study, obtained with the numerical set-up as described afore. At the outset, the flow field

validation will be presented. Afterwards the inclusion of the laser pulse in the numerical simulation shall be discussed and the applied approximation shall be thoroughly detailed. Subsequently, we will dwell on different configurations and examine the relevance of the initial conditions and the distinct features of this test case with respect to its ignitability.

Cold Flow

A cold flow validation was performed by a basic comparison of the PIV (Particle Image Velocimetry) measurements [23] with the results from the CFD simulation. Since the flow field without the presence of droplets is of minor significance for the ignitability and flame behavior from a general perspective, only a single set of conditions was investigated to provide credibility to the flow field results. Figure (5) shows the comparison between experiment and numerical simulation.

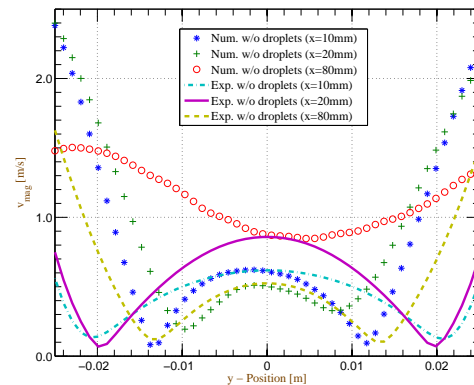


FIGURE 5. Profiles of the cold flow simulation. Boundary conditions as stated in Table 3. The x -value corresponds to the distance from the injector plane. The recirculation zone is much smaller in the experiment due to the unsymmetric inflow which impedes the development of a stable flow field below the injector plane.

Both sets of results exhibit the same features. Moreover, they share the same range of velocities. The major characteristic is the recirculation zone which evolves below the injector plane. The deviations originate from the unsteady behavior of the flow in the experiment which moderates the strength and the extent of the recirculation zone. A different picture establishes, when the dispersed phase is included in the simulation. In Fig. (6), the numerical cold flow results of a stationary steady state calculation with and without droplets are presented.

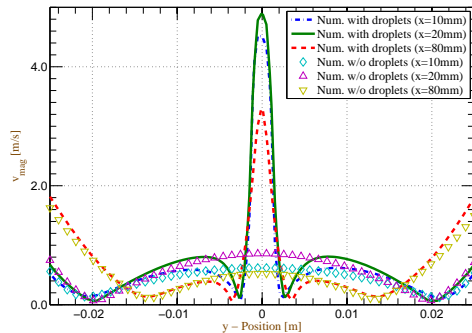


FIGURE 6. Profiles of the cold flow with and without droplets. Boundary conditions as stated in Table 3. The x -value corresponds to the distance from the injector plane.

It is interesting to note the changes in the flow field, which largely influence the ignitability behavior of this set-up. Confined to the middle axis, a jet-like structure appears, which is characterized by a high momentum and contains most of the pre-ignition fuel vapor. The recirculation zone as a consequence has separated to form an outer cylinder surrounding the droplet stream. As the jet spreads during its course further downstream the shear layer becomes less prominent. As no PIV measurement is provided for the cold flow field with dispersed phase, no comparison in terms of velocity agreement can be accomplished. Regarding the cross section area corresponding to the injector holes ($r = 2.23 \text{ mm}$), the droplet mass is exceeding the mass of the continuous phase by a factor of three. This supports the theory that the flow field solution of the cold gas without droplets has only a minor impact. Furthermore, the Stokes Number of the droplets derived with: $St = \rho_L D_d^2 / (18 \mu_g) x (U_d - U_f) / l_r$ (Droplet Velocity: $U_d = 6.5 \text{ m/s}$, Gas Velocity: $U_f = 0.5 \text{ m/s}$, Recirculation length: $l_r = 60 \text{ mm}$) yields droplets with a Stokes Number of > 1 which corresponds to droplets unaffected by the flow field. Thus, on the one hand the droplets are only marginally influenced by the surrounding flow, whereas on the other hand they have a significant impact on the flow field themselves through their mass ratio. Consequently, the effect of the unsymmetry implied by the one-sided inflow condition in the experiment is significantly weak-

ened. This provides credibility to the correctness of the numerical cold flow field for the multiphase run without a data set for comparison. A thorough investigation and validation of the flow features comprising combustion has been carried out in Boyde et al. [8] to which the reader is referred for more details.

Ignition Modeling

The trigger to start the ignition represents still one of the crucial questions of flame propagation modeling. It was observed in the simulation that the influence of the initial ignition kernel in terms of energy and fuel vapor content with respect to the position of the flame in later stages, almost vanishes completely. This severely impairs the validation of new models and, on the other hand, allows the introduction of reasonable simplifications. The work of Bradley et al. [24] on laser pulse ignition has greatly helped the understanding of laser pulse phenomena. It is, however, still beyond the scope of any CFD solver to cope with the complete physics of plasma underlying these processes. Thus, a need for simplified models persists, as for example, employed by Lacaze et al. [6]. The approach applied, so far, is to prescribe an energy source in the domain, to provide the heat to self-ignite the mixture. Regarding the treatment of a multiphase flow, another aspect requires consideration. The vapor content in the laser pulse zone needs to be accounted for, to obtain similar initial conditions as experimentally observed. Since all physical processes, particularly chemical processes and evaporation, are significantly enhanced, a simple approach with solely heating seems questionable. Thus, the energy provided by the laser, which, determined by measurements in the experiment, amounts to approximately 60 mJ, has to be split into two fractions. The first fraction induces the temperature rise, whereas the other part contributes to the rapid release of the vapor. This is depicted schematically in Fig. (7c). It is crucial to begin the simulation with conditions similar to the real laser pulse conditions. Consequently, T_{end} representing the temperature once the plasma state has abated, as illustrated in Fig. (7a) and T_{max} denoting the temperature which is achieved through the heat source, shown in Fig. (7b) need to be of approximately the same magnitude. The same holds for the fuel vapor fraction.

As a consequence of the different nature of the laser-induced spark in general, which is associated with very small time scales and as indicated by the high complexity, induced by the presence of two phases, a further simplification is proposed in this paper. In order to prescribe pseudo-real initial conditions, which serve to mimic the evolution of the initial flame kernel, the experimental data has been assessed and, based on a thorough analysis, some major features have been identified.

1. A large zone encircling the laser pulse focal point is in a reacting state.
2. Fuel vapor has spread out rapidly along the center line.

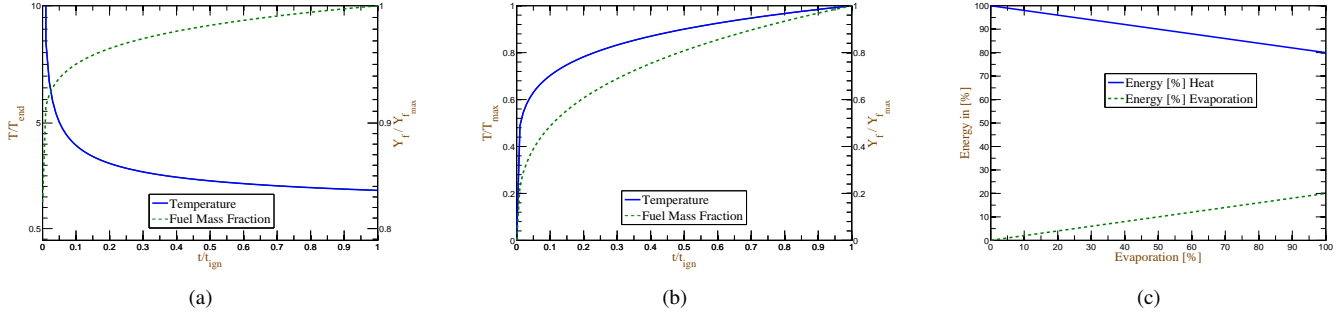


FIGURE 7. Time evolution of temperature and fuel vapor schematically. (a) Real process. (b) Approximated process by a continuous heat source. (c) Principle split of the energy into a heating fraction and an evaporation fraction. Note the difference in the ordinate scale.

The results obtained in the experiment, corresponding to 0.5 ms after the laser pulse event, are presented in Fig. (8). As stated by Bradley et al. [24], due to the creation of radicals in the plasma volume, all processes are significantly accelerated, which leads to an excessive exchange of energy and matter. According to these results and in order to reproduce the experimental findings, the assumptions made to ignite the mixture are a hot zone of 3000 K temperature, mimicking the laser heating and a spontaneous vapor increase are prescribed. Of course, the total energy for both effects is bounded by 60 mJ. This represents the constraint for the numerical ignition. Based on the findings in the experi-

numerical laser volume, is prescribed as a cylinder which is in good accordance to Fig. (8). The radius of the cylinder complies with the dimensions determined experimentally, corresponding to a size of 4 mm. Consequently, the quantity which is varied, is the cylinder height, see Fig. (9). In case a high vapor content is assumed to be induced by the laser pulse, the height is decreased to account for the energy of the vaporisation. Naturally, the more energy is consumed by the evaporation, the less energy is available to generate a large initial hot zone. Table 4 illustrates the split-up. The spark height (l_s is calculated following Eq. (13):

$$E_e + E_h = l_s \cdot (\pi r^2 \cdot (\rho_{\text{ign}} h_{\text{ign}} - \rho_0 h_0) + f_e \cdot H_e \frac{\dot{m}_f}{v_f}), \quad (13)$$

with f_e denoting the fraction of liquid fuel mass contained in the cylinder which evaporates, r , the prescribed radius of 4 mm, h_{ign} , h_0 , ρ_{ign} and ρ_0 the specific enthalpy and density at the corresponding temperatures, respectively. Furthermore, H_e represents the evaporation enthalpy whereas E_e , E_h constitute the evaporation and heating energy. h corresponds to the resulting height of the cylinder, \dot{m}_f to the fuel mass flow rate and v_f to the fuel velocity which is derived from the continuity equation at the injector holes. Note that the computed height and the visible height in Fig. (8) are in good agreement. The further objectives of this study is to prove the validity of the approach and to investigate the behavior of the initial kernel.

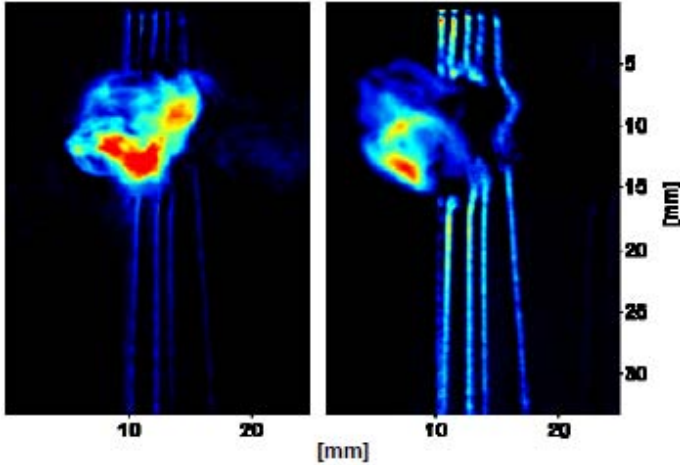


FIGURE 8. Ensemble-averaged images derived in the experiment from 50 measurements. The left hand side shows the fuel concentration, 0.5 ms after the laser pulse event. The right hand side shows the OH concentration. Note that the fuel droplets in the laser zone have almost fully vanished. The height of the gap is approximately 10 mm.

ment, see Mosbach et al. [23], the volume which constitutes the

Per Cent of Fuel (n-Decane) evaporated	Resulting Height
0 [%]	10.68 mm
50 [%]	9.48 mm
100 [%]	8.52 mm

TABLE 4. Resulting heights for different vapor contents.

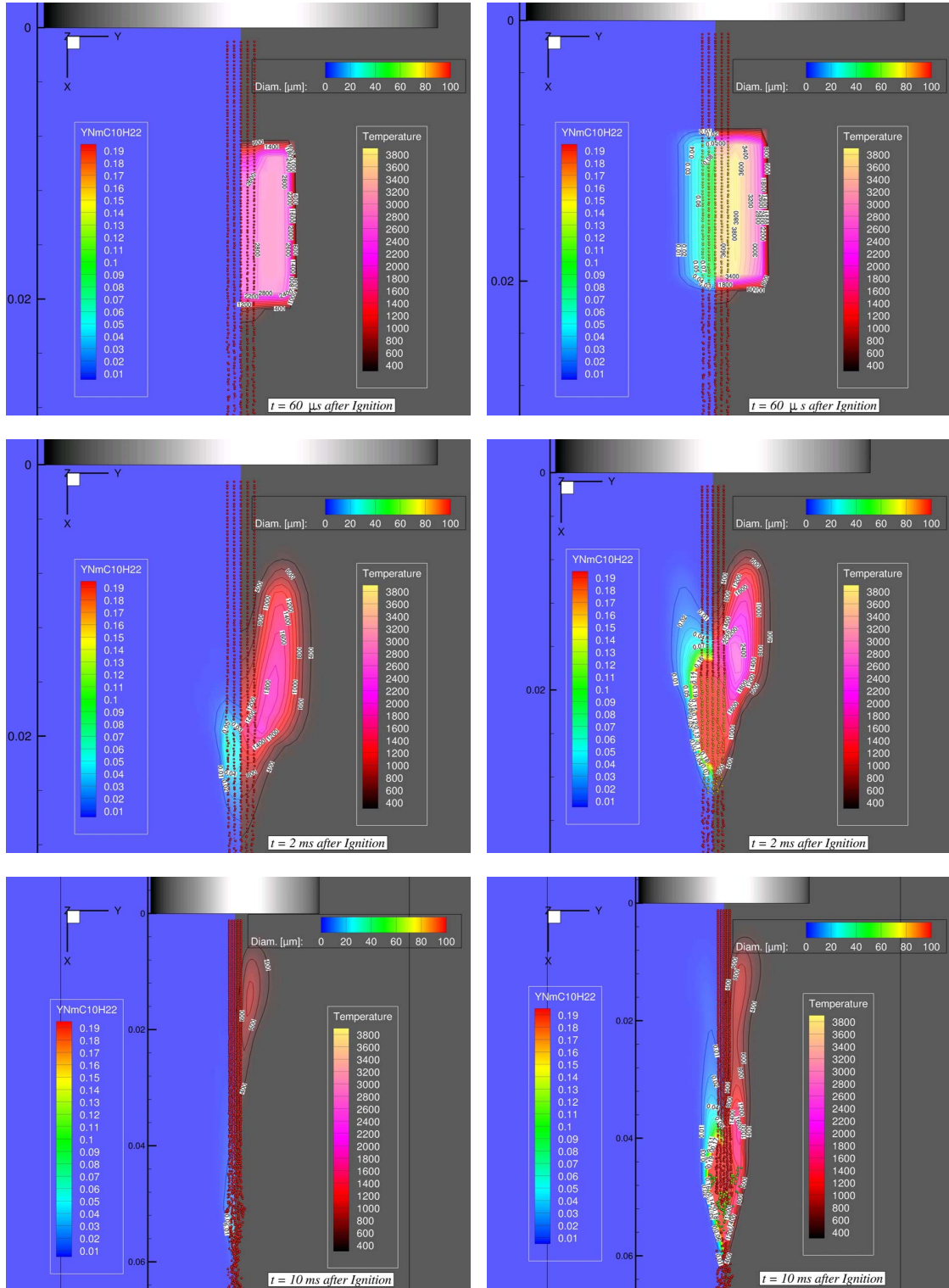


FIGURE 10. Flame and Fuel Evolution triggered with two different ignition settings. Columns: correspond to 0 % vapor / 50 % vapor present in the ignition zone. **Rows:** time passed after laser pulse. 1st Row: 60 μs . 2nd Row: 2 ms. 3rd Row: 10 ms. Note that for 0 % vapor a failed ignition occurs. 50 % vapor leads to a successful ignition and to a self-sustaining flame.

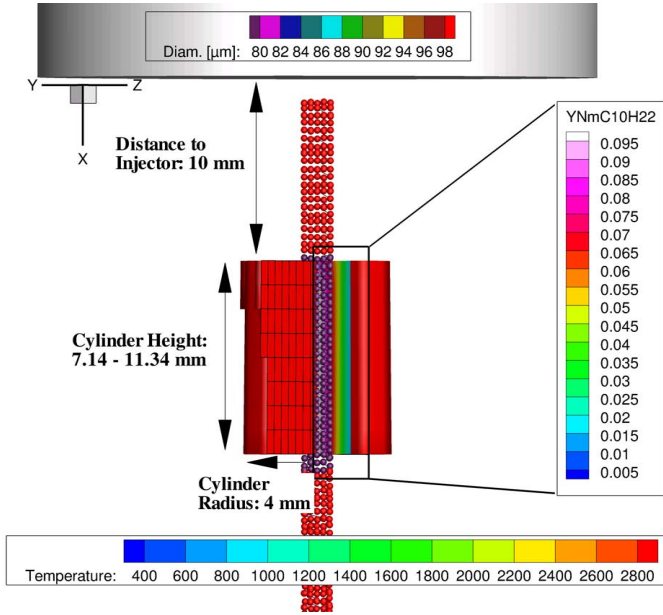


FIGURE 9. Dimensions and set-up of the ignition kernel with $f_e = 0.5$ (50 % of the droplet fuel mass evaporates spontaneously). The top shows the injector plane with the emerging droplets. The red cylinder illustrates the numerical ignition kernel, with the temperature presented on the left side and the fuel vapor mass concentration due to the assumed spontaneous evaporation on the right. The color of the droplets indicates their diameter. Note that the diameter in the ignition kernel is smaller due to the assumed spontaneous evaporation.

Example Ignition

On the basis of a specific set of boundary conditions as listed in Table 3, the differences which occur due to variations in the assumptions made regarding the laser pulse modeling, shall be investigated. This paragraph also serves as an illustration of some major aspects in the design of an ignition device. In Fig. (10) a time series of attempted ignitions is presented, with one ignition leading to the development of a flame, whereas the second one results in a failed ignition. Although both set-ups obtain the same amount of energy, the distribution varies, from, in the first case without initial vapor to 50 % spontaneous evaporation of the droplets present in the cylinder volume. When looking at the averaged position of the fuel vapor concentration and of the flame, as illustrated in Fig. (11), the differences in appearance between both distinctive calculations become more obvious. Note that for the flame center position a density averaging routine of areas with a temperature of above 500 K has been performed. The same procedure has been carried out for a fuel mass fraction above 0.02. In the first scenario, corresponding to the case of zero vapor present in the ignition, the droplets require the full length of the hot zone to start evaporating. Thus, the vapor zone

and the laser pulse region are not aligned, leading to unfavorable conditions and resulting in a failed ignition. In the second configuration, a flame kernel establishes in the initial vapor concentration, counteracting the dissipation and convection of the laser pulse energy. In the third case, not presented here, regarding an initial evaporation of 100 % of the droplets, the path length of hot gas, although it involves enough fuel vapor, is too short for the incoming fuel droplets, to evaporate sufficiently to sustain the flame. Therefore, two different causes for a failed ignition have been identified. A too confined prescribed laser pulse region can result in a failed ignition and, secondly, a set-up in which the fuel vapor and the hot zone are displaced.

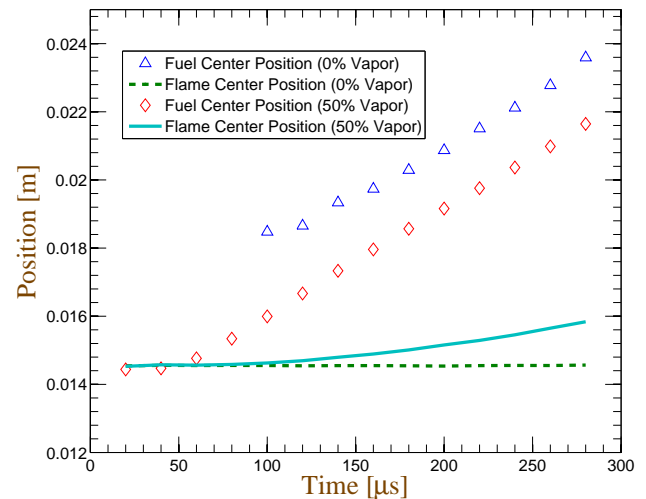


FIGURE 11. Fuel and flame center positions correlated with the simulation time. Boundary conditions as stated in Table 3. The x -value corresponds to the distance from the injector plane.

Ignition Map

In order to examine the numerical laser ignition model, with respect to its capability of reproducing the experimental results, the ignition map, depicted in Fig. (12), is used as a benchmark. The parameters for the laser ignition model are varied in order to provide the best accordance. The numerical results are also presented in Fig. (12). The fuel employed in this set-up is Jet A-1. In the numerical simulations, kerosene is modeled on the liquid phase as detailed in Table 2 as a CTM fuel. With this surrogate fuel for kerosene very reasonable results were obtained in terms of evaporation characteristics, see Le Clercq et al. [22]. In the gas phase, the fuel is modeled as single component n-Decane fuel vapor which is regarded as a valid approximation, since the fuel velocities obtained with the coefficients from Table 1 match closely the experimental laminar flame speed data

derived by Eberius et al. [25] for kerosene. Figure (12) presents the final outcome of a numerically obtained ignition map. The parameters for the ignition kernel for this plot correspond to 0 % vapor in the ignition kernel zone. From numerous simulations the

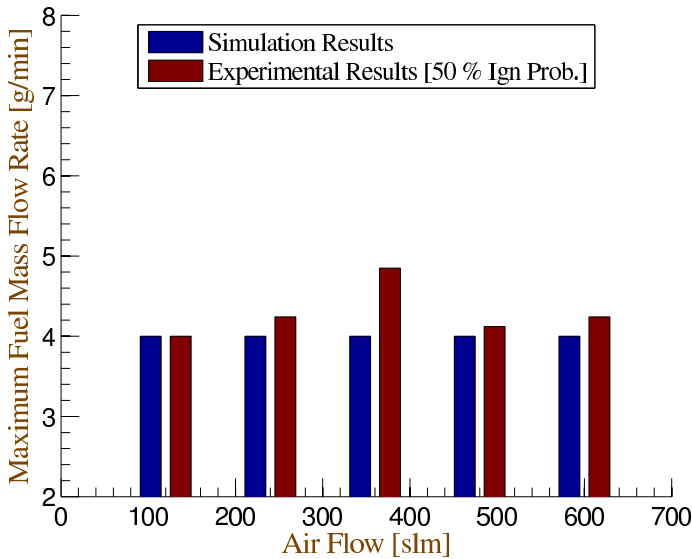


FIGURE 12. Ignition probability map. Experimental statistics are obtained from 10 different ignition events. The threshold for the comparison corresponds to 50 % ignition probability for the experimental results. Numerical results were gained with 0 % initial vapor present in the ignition kernel.

most realistic ignition parameters for a multiphase flow simulation could be obtained. The best compliance to the experimental data was achieved when using 0 % vapor in the ignition kernel which, consequently, resulted in a larger initial hot zone. Moreover it appeared in the course of this work, that the time delayed creation of fuel vapor is a crucial aspect of the ignition procedure which largely controls the ignitability. The outcome shows, that the evaporation caused by the high temperatures in the ignition kernel provides enough fuel vapor for an initial flame kernel to develop. When imposing 50 % fuel vapor in the ignition kernel, the ignitability with respect to the maximum fuel mass flow rate significantly increases beyond the range which was identified in the experimental study. The limits of ignitability are listed in Table 5.

% Vapor	0	50	100
Max. Fuel Mass Flow Rate (Jet A-1) [g/min]	4.0	6.5	6.0

TABLE 5. Maximum fuel mass flow rates, for which a successful ignition can be accomplished, correlated with the ignition vapor content for an air mass flow of 300 slm (standard liter per minute).

The numerically derived ignition map does not exhibit the small deviations in the ignitability as observed in the experimental study. The reasons for the fluctuations can stem from the unsymmetric inflow conditions imposed on the experiment, which can cause stronger flow structures in front of the injector plane and hence, lead to statistic differences. Consequently, each inflow condition has its characteristic flow field which slightly affects the results. The outcome only varies in the range of tenth of percent which are difficult to resolve with a URANS simulation with a constant inflow prescribed. From a general perspective, however, the agreement between the numerically determined and experimental ignition limits is very satisfying and supports the chosen modeling approach.

The second factor which was more closely investigated relates to the differences in the liquid property models. For all previous simulations the CTM model was applied, which predicts a more realistic evaporation of the fuel, as a distribution of different species is assumed and, hence, the more volatile components are incorporated. Opposed to that, by modeling the fuel as a single component fuel, deviations occur, as the vaporisation is underestimated. This was carried out for the benchmark set-up of a 300 slm air inlet boundary condition, which resulted in a maximum ignitable fuel mass flow rate of 3.5 g/min. As measurements prove, that higher fuel mass flow rates are possible, this points out, that a better agreement can be achieved by employing sophisticated evaporation models.

Conclusion

A numerical set-up was presented which is able to model ignition phenomena in a multiphase flow environment. The validation, which was performed in Boyde et al. [16], demonstrates that all employed models provide a very good accuracy in terms of resolving the flame position in general and flame spreading more specifically. Thus, the focus in this study was placed on the initial stages of the ignition process, namely, the inclusion of the laser-induced spark. This was accomplished by prescribing an energy source for the domain which was split into a part for the spontaneous evaporation of the enclosed droplets and the heating of the corresponding volume. Both parameters, hence, the total energy and the energy split factor are key parameters concerning the ignition process observed in the simulation. The study has pointed out, that huge differences regarding the ignitability

of a configuration can occur when varying the ignition parameter with respect to the vapor content in the initial kernel. Consequently, in order to identify the correct settings an ignition map was generated, on which grounds the most reliable set of parameters could be determined. The parameter investigation has revealed, that although physical processes are significantly enhanced by the laser ignition, the numerical modeling achieves the best agreement with no initial fuel vapor concentration assumed. Moreover, it was demonstrated that an additional spontaneous vaporisation of droplets leads to excessive favorable conditions which results in an over prediction of the ignition probabilities. It was also highlighted that the fuel evaporation is of high relevance. The single component modeling of Jet A-1 yielded an under prediction of the ignition probability, whereas the simulation agreed well with the experimental data set when applying the CTM approach, as a more sophisticated model. With the derived parameters, the TFC model with its laser ignition extension was validated for multi-phase flow set-ups and can be utilised in further applications. For similar configurations it needs to be evaluated to which extent the vapor content in the ignition zone has a universal character and whether an optimum vapor content and amount of energy can be identified which yields an equivalent ignition behavior as observed experimentally.

ACKNOWLEDGMENTS

The authors greatly acknowledge the valuable work of the researchers at the Lab Scale experiment. This work received funding from the European Community through the project TIMECOP-AE (Project # AST5-CT-2006-030828). It reflects only the author's views and the Community is not liable for any use that may be made of the information contained therein.

REFERENCES

- [1] Birch, A. D., Brown, D. R., and Dodson, M. G., 1981. "Ignition probabilities in turbulent mixing flows". *Proceedings of the Combustion Institute*, **18**, pp. 1775–1780.
- [2] Ahmed, S. F., and Mastorakos, E., 2006. "Spark ignition of lifted turbulent jet flames". *Combustion and Flame*, **146**, pp. 215–231.
- [3] Ahmed, S. F., Balachandran, R., Machione, T., and Mastorakos, E., 2007. "Spark ignition of turbulent nonpremixed bluff-body flames". *Combustion and Flame*, **151**, pp. 366–385.
- [4] Ahmed, S. F., Bahane Ledezma, I. A., and Mastorakos, E., 2009. "Spark ignition in a turbulent shearless fuel-air mixing layer: Average flame growth rates". *47th American Institute of Aeronautics and Astronautics Science Meeting*.
- [5] Mastorakos, E., 2008. "Ignition of turbulent non-premixed flames". *Progress in Energy and Combustion Sciences*, pp. 1–40.
- [6] Lacaze, G., Richardson, E., and Poinso, T., 2009. "Large eddy simulation of spark ignition in a turbulent methane jet". *Combustion and Flame*, **156**, pp. 1993–2009.
- [7] Boyde, J. M., Di Domenico, M., Noll, B. E., and Aigner, M., 2010. "Spark ignition simulations and the generation of ignition maps by means of a turbulent flame speed closure approach". *ASME*.
- [8] Boyde, J. M., Le Clercq, P., Di Domenico, M., Mosbach, T., Gebel, G., Rachner, M., and Aigner, M., 2011. "Ignition and flame propagation along planar monodisperse droplet streams". *AIAA Aerospace Sciences Meeting and Exhibit*.
- [9] Ferziger, J. H., and M., P., 2008. *Numerische Stroemungsmechanik*. Springer-Verlag.
- [10] Pope, S. B., 2000. *Turbulent Flows*. Cambridge University Press.
- [11] Saad, Y., 2003. *Iterative methods for sparse linear systems*. Society for Industrial and Applied Mathematics, Philadelphia, USA.
- [12] Zimont, V. L., 1979. "Theory of turbulent combustion of homogeneous fuel mixtures at high reynolds numbers". *Fizika Goreniya i Vzryva*, **15**, pp. 23–32.
- [13] Durand, L., 2007. "Development, implementiaton and validation of les models for inhomogeneously premixed turbulent combustion". PhD thesis, University of Munich.
- [14] Polifke, W., Flohr, P., and Brandt, M., 2002. "Modeling of inhomogeneously premixed combustion with an extended tfc model". *ASME*, **124**, pp. 58–65.
- [15] Zimont, V. L., and Lipatnikov, A. N., 1995. "A numerical model of premixed turbulent combustion of gases". *Chemical Physical Reports*, **14**, pp. 993–1025.
- [16] Boyde, J. M., Fiolitakis, A., and Di Domenico, M. and Aigner, M., 2011. "Correlations for the laminar flame speed, adiabatic flame temperature and ignition delay time for methane, ethanol and n-decane". *AIAA Aerospace Sciences Meeting and Exhibit*.
- [17] Bluemcke, E., 1992. "Turbulente partikeldispersion in eingeschlossenen drallstroemungen". PhD thesis, DLR, German Aerospace Center, Institute of Propulsion Technology.
- [18] Le Clercq, P. C., and Bellan, J., 2004. "Direct numerical simulation of a transitional mixing layer laden with multicomponent-fuel evaporating drops using continuous thermodynamics". *Journal of Phys. Fluids*, **16**, pp. 1884–1907.
- [19] Le Clercq, P. C., and Bellan, J., 2005. "Direct numerical simulation of gaseous mixing layers laden with multicomponent-fuel-liquid drops: liquid specific effects". *Fluid Mech*, **533**, pp. 57–94.
- [20] Le Clercq, P., Doue, N., Rachner, M., and Aigner, M., 2009. "Validation of a multicomponent-fuel model for spray computation". *Proceedings of the 47th AIAA Aeropsace Sciences Meeting*.

- [21] Wahl, C., 2003. Eu fp5 g4rd-ct-00075 final report. Tech. rep., DLR, German Aerospace Center, Institute of Combustion Technology.
- [22] Le Clercq, P., Di Domenico, M., Rachner, M., Ivanova, E., and Aigner, M., 2009. "Impact of fischer-tropsch fuels on aero-engine combustion performance". *AIAA*.
- [23] Mosbach, T., and Gebel, G., 2010. Report on the experiments at the lab-scale combustor (d2.2.3b). Tech. rep., TIMECOP-AE Project no: AST5-CT-2006-030828.
- [24] Bradley, D., Sheppard, C. G. W., Suardjaja, I. M., and Woolley, R., 2009. "Fundamentals of high-energy spark ignition with lasers". *Combustion and Flame*, **156**, pp. 55–77.
- [25] Eberius, H., Frank, P., Kick, T., Naumann, C., and Steil, C., 2001. Final report for subtask 1.2.3 (d1.7). Tech. rep., EU project computational fluid dynamics for combustion No. grd1-1999-10325.